A&A 492, 93–99 (2008)
DOI: 10.1051/0004-6361:200810674
© ESO 2008

Astronomy & Astrophysics

The efficient low-mass Seyfert MCG–05–23–016*

V. Beckmann[1,2,3], T. J. -L. Courvoisier[1,2], N. Gehrels[4], P. Lubiński[1,5], J. Malzac[6], P.-O. Petrucci[7], C. R. Shrader[4], and S. Soldi[1,2]

[1] ISDC Data Centre for Astrophysics, Chemin d'Écogia 16, 1290 Versoix, Switzerland
e-mail: Volker.Beckmann@unige.ch
[2] Observatoire Astronomique de l'Université de Genève, Chemin des Maillettes 51, 1290 Sauverny, Switzerland
[3] University of Maryland Baltimore County, 1000 Hilltop Circle, Baltimore, MD 21250, USA
[4] Astrophysics Science Division, NASA Goddard Space Flight Center, Code 661, MD 20771, USA
[5] Centrum Astronomiczne im. M. Kopernika, Bartycka 18, PL-00-716 Warszawa, Poland
[6] Centre d'Étude Spatiale des Rayonnements (CESR), OMP, UPS, CNRS, BP 44346, 31028 Toulouse Cedex 4, France
[7] Laboratoire d'Astrophysique de Grenoble, Univ. J. Fourier/CNRS, UMR 5571, BP 53X, 38041 Grenoble Cedex, France

Received 25 July 2008 / Accepted 10 October 2008

ABSTRACT

Aims. The Seyfert 1.9 galaxy MCG–05–23–016 has been shown to exhibit a complex X-ray spectrum. This source has moderate X-ray luminosity, hosts a comparably low-mass black hole, but accretes at a high Eddington rate, and allows us to study a super massive black hole in an early stage.

Methods. Three observations of the INTEGRAL satellite simultaneous with pointed Swift/XRT observations performed from December 2006 to June 2007 are used in combination with public data from the INTEGRAL archive to study the variability of the hard X-ray components and to generate a high-quality spectrum from 1 to 150 keV.

Results. The AGN shows little variability in the hard X-ray spectrum, with some indication of a variation in the high-energy cut-off energy ranging from 50 keV to $\gg$100 keV, with an electron plasma temperature in the 10–90 keV range. The reflection component is not evident and, if present, the reflected fraction can be constrained to $R < 0.3$ for the combined data set. Comparison to previous observations shows that the reflection component has to be variable. No variability in the UV and optical range is observed on a time scale of 1.5 years.

Conclusions. The hard X-ray spectrum of MCG–05–23–016 appears to be stable with the luminosity and underlying power law varying moderately and the optical/UV flux staying constant. The reflection component and the iron Kα line seem to have decreased between December 2005 and the observations presented here. The spectral energy distribution appears to be similar to that of Galactic black hole systems, e.g. XTE 1118+480 in the low state. The AGN exhibits a remarkably high Eddington ratio of $L_{\rm bol}/L_{\rm Edd} \gtrsim 0.8$ (or $L_{\rm bol}/L_{\rm Edd} \gtrsim 0.1$, if we consider a higher mass of the central engine) and, at the same time, a low cut-off energy around 70 keV. Objects like MCG–05–23–016 might indicate the early stages of super massive black holes, in which a strong accretion flow feeds the central engine.

Key words. galaxies: active – galaxies: Seyfert – X-rays: galaxies – galaxies: individual: MCG–05–23–016 – accretion, accretion discs

1. Introduction

Active galactic nuclei (AGN) are commonly assumed to be super massive black holes in the centre of galaxies, in which accretion processes give rise to emission throughout the electromagnetic spectrum. AGN are observed to date up to redshifts of $z \sim 6.4$ (Willott et al. 2007), showing that super massive black holes with masses of $M_{\rm BH} \sim 10^8\ M_\odot$ must have been formed as early as <0.7 Gyrs after the formation of the first stars (Kashlinsky et al. 2005). In order to be able to form super massive black holes at this early stage of the Universe, merging events and high accretion rates are required. This black hole evolution is closely tied to the growth of the bulge of the AGN's host galaxy, as both seem to be correlated with $M_{\rm BH} \simeq 10^{-3}\ M_{\rm Bulge}$ (Gebhardt et al. 2000).

Recent studies intend to not only find unification models for the different AGN types but also probe whether their central engines and super massive black holes are simply up-scaled versions of Galactic black holes like Cyg X–1, GRO J1655–40, or GX 339–4. In this context, models of black hole accretion can be tested using objects showing extreme physical properties, like luminosity, accretion rate, or Eddington ratio. The Seyfert 1.9 galaxy presented here resides in an extreme end of the known parameter space of AGN. X-ray observations give a direct view on matter close to the super massive black hole, providing insights into the geometry and the state of the matter. The flux and spectral variability of the sources in the hard X-rays reflect the size and physical state of the regions involved in the emission processes (see Uttley & McHardy 2004, for a brief review).

MCG–05–23–016 is one of the brightest Seyfert galaxies in the X-rays. This Seyfert 1.9 galaxy at redshift $z = 0.0085$ has not only been studied in the 2–10 keV band by most X-ray missions so far, but has also been detected in hard X-rays above 20 keV with *BeppoSAX*/PDS (e.g. Balestra et al. 2004), *INTEGRAL*/IBIS (Soldi et al. 2005), and *Swift*/BAT

* Based on observations with INTEGRAL, an ESA project with instruments and science data centre funded by ESA member states (especially the PI countries: Denmark, France, Germany, Italy, Switzerland, Spain), Czech Republic and Poland, and with the participation of Russia and the USA.

Table 1. Observation log of *INTEGRAL* and *Swift*/XRT observations on MCG–05–23–016.

INTEGRAL revolution	Time covered U.T.	ISGRI exposure [ks]	JEM-X exp. [ks]	Swift/XRT U.T.	Exposure [ks]
256–282	04–11–18 – 05–02–05	69.3	–	05–12–09	10.3
508	06–12–12–06–12–13	26.3	21.7	06–12–13	1.9
565	07–05–30–07–06–01	128.7	122.0	07–05–31	2.1
569	07–06–12–07–06–13	89.4	79.8	07–06–13	2.9

(Beckmann et al. 2007; Tueller et al. 2008). With a bolometric luminosity of $L_{\rm bol} \simeq 2 \times 10^{44}$ erg s^{-1} this Seyfert is a moderately luminous object, with a comparably small central black hole of $M_{\rm BH} = 2 \times 10^6\ M_\odot$ (Wang & Zhang 2007). Wang & Zhang used the width of the OIII line (Greene & Ho 2005) to obtain the black hole mass from the $M_{\rm BH}$–σ relation (Tremaine et al. 2002) and give the error of the measurement with 0.7 dex.

Balestra et al. (2004) derived from *ASCA*, *BeppoSAX*, *Chandra* and *XMM-Newton* data that the iron Kα line apparent in the spectrum seems to be a superposition of a narrow and a broad component, that a reflection component of $R = 0.45$ is detectable, and that the continuum can be modeled by a photon index of $\Gamma \simeq 1.7$ and a cut-off at $E_{\rm C} = 110$ keV. The observations covered a time span from 1994 to 2001, during which the object showed little flux variation and a stable spectrum as well as constant iron line and reflection component. A recent re-analysis of the *BeppoSAX* data by Dadina (2007) indicates a slightly steeper spectrum ($\Gamma = 1.79^{+0.07}_{-0.08}$) with higher cut-off energy ($E_{\rm c} = 191^{+110}_{-60}$ keV), and stronger reflection component ($R = 0.74^{+0.22}_{-0.52}$). An analysis of *RXTE* data by Mattson & Weaver (2004) using a fixed underlying power law slope of $\Gamma = 1.88$ led to a variable reflection component in the range $R = 0.35$–0.57 and iron $K\alpha$ line flux ($f_{K\alpha} = (1.55-1.99) \times 10^{-4}$ photons keV^{-1} cm^{-2} s^{-1}). Recently, observations on MCG–05–23–016 by *Suzaku* showed a 0.4–100 keV spectrum which appeared to be a cut-off power law of $\Gamma = 1.9$ and $E_{\rm C} > 170$ keV plus a dual reflector with $R \sim 0.9$ and $R \sim 0.5$, respectively (Reeves et al. 2007). *XMM-Newton* and *Chandra* data confirmed that the iron Kα line complex consists of a broad and of a narrow component and revealed evidence for outflowing material (Braito et al. 2007). The exact shape and structure of the high-energy spectrum of MCG–05–23–016 remains elusive though. *INTEGRAL* and *Swift* observations can help to shed light on the existence and position of the high-energy cut-off and variability of the hard X-ray spectrum. In Sect. 2 we describe the analysis of the *INTEGRAL* and simultaneous *Swift* observations. We discuss the findings in Sect. 3, with emphasis on similarities with Galactic black hole systems and on the fact that the Seyfert galaxy apparently operates at high Eddington ratio. Conclusions are presented in Sect. 4.

2. Observations and data analysis

The *INTEGRAL* (Winkler et al. 2003) mission offers the unique possibility to perform simultaneous observations of AGN over the 3–1000 keV energy region. This is achieved by the X-ray monitor (3–35 keV) JEM-X (Lund et al. 2003), the soft gamma-ray imager (18–1000 keV) IBIS/ISGRI (Lebrun et al. 2003), and the spectrograph SPI (Vedrenne et al. 2003), which operates in the 20–8000 keV region. Each of these instruments employs the coded-aperture technique.

INTEGRAL performed three dedicated pointed observations on MCG–05–23–016 in December 2006 (spacecraft revolution 508) and in May/June 2007 (revolution 565 and 569). As observing strategy hexagonal dithering has been chosen in order to achieve a sufficient coverage also by the JEM-X monitor. During these observations the spectrometer SPI was not available because it went through an annealing cycle. In addition and for comparison reasons, we analysed *INTEGRAL* data on MCG–05–23–016 which had been taken prior to our observations. During all these measurements the source was too far off-axis to be covered by JEM-X. Reliable data from the SPI spectrometer can be taken also at larger off-axis angles. Therefore the public SPI data include more revolutions than the IBIS/ISGRI data analysed here. All *INTEGRAL* data were analysed using the Offline Science Analysis (OSA) software version 7.0 distributed by the ISDC (Courvoisier et al. 2003). For IBIS/ISGRI standard spectral extraction was applied, using 12 spectral bins in the 18 keV to 521 keV energy range. For JEM-X the flux values were extracted from imaging analysis in four energy bands (3–6–10–15–35 keV), which provides more reliable results for a source at the flux level of MCG–05–23–016 than standard spectral extraction.

In order to achieve a wider spectral energy coverage, pointed *Swift* observations were performed simultaneous with the *INTEGRAL* ones. *Swift* (Gehrels et al. 2004) provides two narrow-field instruments, the XRT (Burrows et al. 2005) with energy range 0.3–10.0 keV and the UVOT (Roming et al. 2005) which is equipped with 6 filters in the optical and UV range. The XRT and UVOT data have been analysed using HEADAS version 6.1.1 applying latest calibration files as available in January 2008.

The *INTEGRAL* IBIS/ISGRI and JEM-X1, as well as the *Swift* pointed observations are summarised in Table 1. The observations in *INTEGRAL* revolution 508, 565, and 569 are truly simultaneous with *Swift* pointed observations, while the public data obtained from revolution 256 to 282 are separated from the *Swift* observation by at least 10 months and also do not include any JEM-X data and therefore no information about the 9–18 keV energy range. The SPI data showed only a marginal detection on the 4σ level in the 20–40 keV energy band in the combined data set. The SPI spectrum can be fit by a single power law model with photon index $\Gamma = 1.8^{+1.5}_{-0.6}$[1]. As these data are not strictly simultaneous with the other observations and are of low significance, the SPI data have not been considered in the following analysis of MCG–05–23–016.

The data of IBIS/ISGRI, JEM-X, and Swift/XRT have been fit simultaneously using XSPEC version 11.3.2 (Arnaud 1996). As the most simplistic approach an absorbed power law model has been fit to the data. Only in the case of revolution 508 data this model gives an acceptable fit with $\chi^2_\nu = 1.06$ for 55 degrees of freedom. In the other cases, a good fit was achieved

[1] Errors are 2σ errors throughout the paper.

Table 2. Spectral fitting of combined *Swift*/XRT and INTEGRAL ISGRI/JEM-X1 data of MCG–05–23–016 using an absorbed cut-off power law model.

INTEGRAL revolution	$N_{\rm H}$ [10^{22} cm^{-2}]	Γ	$E_{\rm C}$ [keV]	χ^2_ν	d.o.f.
256–282	$1.26^{+0.07}_{-0.07}$	$1.49^{+0.08}_{-0.08}$	57^{+31}_{-16}	1.05	276
508	$1.29^{+0.15}_{-0.14}$	$1.76^{+0.08}_{-0.08}$	>90	1.06	55
565	$1.24^{+0.14}_{-0.13}$	$1.51^{+0.09}_{-0.10}$	86^{+68}_{-29}	0.95	80
569	$1.04^{+0.10}_{-0.09}$	$1.42^{+0.09}_{-0.09}$	65^{+35}_{-18}	0.92	97
all data	$1.24^{+0.05}_{-0.05}$	$1.52^{+0.07}_{-0.05}$	72^{+21}_{-14}	0.99	268

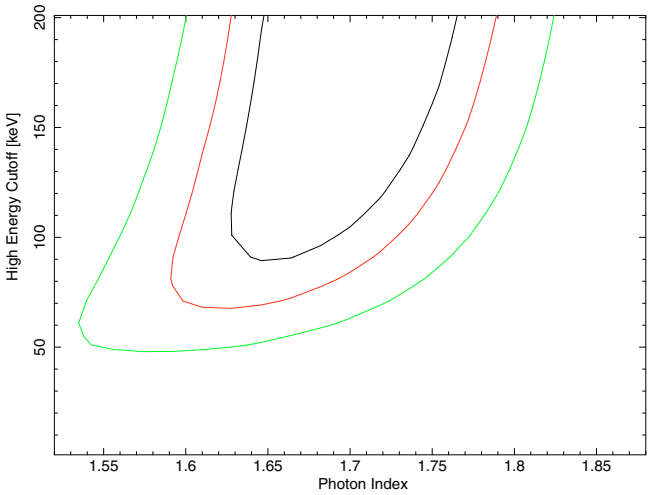

Fig. 1. Contour plot for an absorbed cut-off power law applied to the combined *Swift*/XRT, *INTEGRAL* JEM-X1, and IBIS/ISGRI data obtained in December 2006. The contours show the allowed range for the photon index and the cut-off energy at the 1, 2 and 3 sigma level. No cut-off is required by the data.

with an absorbed cut-off power law model. The fit results are summarised in Table 2.

All spectra require a high-energy cut-off in the range 60–85 keV. The only exception is the short exposure in revolution 508. In this case, the existence of a cut-off at 50 keV, 70 keV and 90 keV, can be rejected at a significance level of 3σ, 2σ, and 1σ, respectively, as shown in Fig. 1.

None of the spectra required an additional reflection component. Applying a Compton reflection model, such as `pexrav` (Magdziarz & Zdziarski 1995) which describes a reflection component from cold material using a cut-off power-law as continuum, shows that the existence of such a component in MCG–05–23–016 can neither be proven nor rejected by the single spectra. The soft X-ray excess below 0.8 keV, as reported in Reeves et al. (2007), is apparent only in *Swift*/XRT spectrum of December 2005.

As the spectral parameters listed in Table 2 appear to be nearly constant, we also applied a fit to the total combined data set as shown in Fig. 2. The total combined spectrum can be fit by an absorbed cut-off power law model with $N_{\rm H} = (1.24 \pm 0.05) \times 10^{22}$ cm^{-2}, photon index $\Gamma = (1.52 \pm 0.05)$, cut-off energy $E_{\rm c} = 72^{+21}_{-14}$ keV. The fit results in $\chi^2_{268} = 0.99$. The significance of the high energy cut-off and the tight constraint on the spectral slope can be seen in the contour plot shown in Fig. 3. For this combined spectrum also the strength of a possible Compton reflection component can be constrained. Applying the `pexrav` model and using the same relative iron abundance

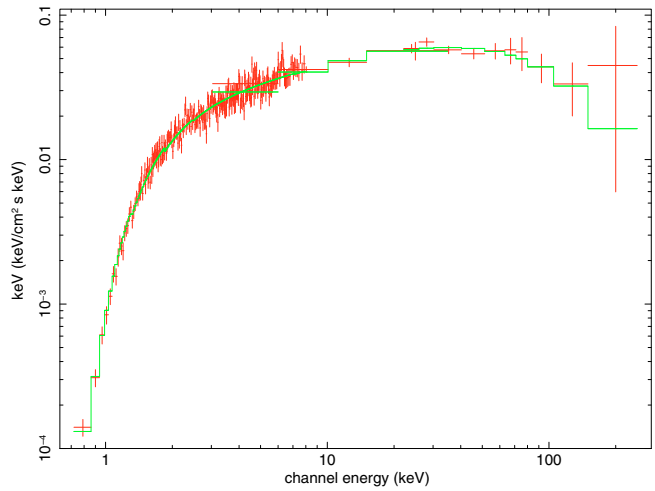

Fig. 2. Combined spectrum of all *Swift*/XRT, *INTEGRAL* JEM-X1, and IBIS/ISGRI data obtained between November 2004 and June 2007. The absorbed cut-off power law fit results in $N_{\rm H} = (1.24 \pm 0.05) \times 10^{22}$ cm^{-2}, photon index $\Gamma = 1.52 \pm 0.05$, and cut-off energy $E_{\rm c} = 72^{+21}_{-14}$ keV for a $\chi^2_{268} = 0.99$.

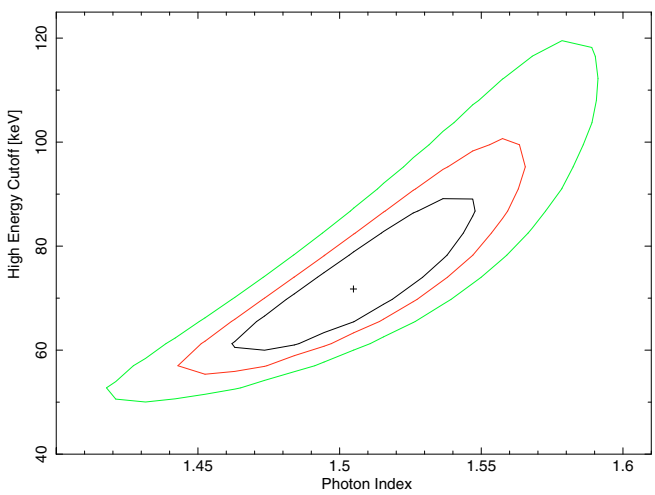

Fig. 3. Contour plot for an absorbed cut-off power law applied to all the combined *Swift*/XRT, *INTEGRAL* JEM-X1, and IBIS/ISGRI data listed in Table 1. The contours show the allowed range for the photon index and the cut-off energy at the 1, 2 and 3 sigma level.

of 0.4 and inclination angle of 45° as Reeves et al. (2007) result in similar absorption, photon index and cut-off energy ($N_{\rm H} = 1.25^{+0.06}_{-0.05} \times 10^{22}$ cm^{-2}, $\Gamma = 1.52^{+0.07}_{-0.05}$, $E_{\rm f} = 72^{+21}_{-14}$ keV), and gives a relative reflection strength of $R = 0.06^{+0.20}_{-0.06}$ ($\chi^2_{267} = 0.99$). The `compPS` model developed by Poutanen & Svensson (1996) for a plane-parallel slab geometry using exact numerical solution of the radiative transfer equation indicates a stronger reflection component ($R = 0.4^{+0.3}_{-0.2}$ with an electron temperature of $kT_{\rm e} = 113^{+15}_{-10}$ keV ($\chi^2_{265} = 1.04$). It has to be pointed out though that this model is a significantly worse representation of the data than the `pexrav` or the simple cut-off power law model. Thus, also in the overall combined spectrum a reflection component is not required, and can be constrained to $R < 0.25$ on a 2σ level. Adding a Gaussian line at the position of the FeK$_\alpha$ line gives an equivalent width of $EW = 61^{+47}_{-40}$ eV, although this component is not statistical significant.

We then left the iron abundance as a free parameter in the `pexrav` model and forced the iron line flux to have an equivalent

width of 100 eV with respect to the reflection continuum alone. Applying this model, one finds that the iron abundance is not constrained by the data and one gets similar results with a marginal evidence for a reflection component of $R = 0.13^{+0.18}_{-0.13}$ consistent with no reflection, a cut-off energy of $E_f = 77^{+17}_{-18}$ keV, and photon index $\Gamma = 1.56^{+0.05}_{-0.09}$ ($\chi^2_{265} = 1.02$).

The *Swift* pointed observations also provide flux information about the UV and the optical V, B, and U bands. All four *Swift*/UVOT measurements revealed the same fluxes within the error of 0.1 mag. The results were: $V = 13.9$ mag, $B = 14.9$ mag, $U = 15.3$ mag, $UVW1 = 16.1$ mag, $UVM2 = 17.0$ mag, and $UVW2 = 16.9$ mag.

2.1. Detection of 1RXS J092418.0–314212

Within the JEM-X data set covering the 3–35 keV energy range, another source is clearly detected in the field of view during the observation of MCG–05–23–016. The source position coincides with 1RXS J092418.0–314212, currently an unidentified object. The source is not detectable in the IBIS/ISGRI data set and the source position is not within the *Swift*/XRT field of view. The JEM-X data cannot be represented by a power law model, but are well represented by a blackbody model with temperature $kT = 1.4^{+0.3}_{-0.2}$ keV. We therefore suggest that this source is likely to be a Galactic X-ray binary system and that the spectrum shows the black body radiation emitted from the central parts of its accretion disc.

3. Discussion

3.1. The hard X-ray emission

In our study of MCG–05–23–016 we have made use of the hard X-ray capabilities of *INTEGRAL*, and in particular of the imager IBIS/ISGRI, in combination with the soft X-ray spectrum provided by *Swift*/XRT. Although the combined spectrum clearly does not provide the wealth of information in the soft X-rays as shown in *XMM-Newton*, *Chandra*, and *Suzaku* data, the better sensitivity at energies above 30 keV puts significant constraints on the hard X-ray component. First of all, a high-energy cut-off in the range 57 keV to 86 keV is required in most of the observed spectra. However, one observation in December 2006 shows a spectrum extending up to ~200 keV, excluding a cut-off at 50 keV on a 3σ level, and at 90 keV on a 1σ level, even when allowing for a different photon index of the underlying power law at the same time (Fig. 1). It is important to note though, that the spectrum in this case is significantly steeper ($\Gamma = 1.7 \pm 0.1$) than in the cases where a cut-off is measured ($\Gamma = 1.5 \pm 0.1$).

The differences in the hard X-ray spectrum, i.e. the differences in high-energy cut-off and spectral slope, can be interpreted as different temperatures of the electron plasma, which is the source of the inverse Compton emission thought to be the dominant component in this energy range. A physical model describing Comptonization of soft photons by a hot plasma, the so called `compTT` model, has been developed by (Titarchuk 1994). The model includes the plasma temperature T_e of the hot corona, the optical depth τ_p of this plasma, and the temperature T_0 of the soft photon spectrum. Because the spectrum starts at $E \simeq 0.7$ keV, T_0 is not well constrained by the data and has been fixed to 10 eV. Table 3 gives the results of this model for the individual data sets as well as for the combined spectrum for plane geometry. As for the cut-off energy E_C, the variation of the plasma temperature is significant on a 2σ level. The highest plasma temperature and lowest optical depth is observed during revolution 508, when the cut-off in the hard X-ray spectrum disappeared (Table 2). However, it has to be taken into account that the rev. 508 spectrum can also be fit by applying the same `compTT` model which gives the best fit to all data (i.e. with $kT_e = 18$ keV and $\tau_p = 2.5$) with an acceptable fit result ($\chi^2_\nu = 1.09$ for 52 d.o.f.).

Table 3. Thermal Comptonisation model (compTT) applied to combined MCG-05-23-016 data.

INTEGRAL revolution	N_H [10^{22} cm^{-2}]	kT_e [keV]	τ_p	L_{2-100} keV [erg s^{-1}]	χ^2_ν	d.o.f.
256–282	$1.33^{+0.07}_{-0.07}$	11^{+15}_{-3}	$3.4^{+0.8}_{-1.0}$	4.3×10^{43}	1.08	275
508	$1.21^{+0.13}_{-0.11}$	90^{+76}_{-73}	$0.5^{+2.4}_{-0.4}$	4.6×10^{43}	0.97	49
565	$1.35^{+0.11}_{-0.11}$	23^{+105}_{-7}	$2.1^{+0.6}_{-1.8}$	4.2×10^{43}	0.91	79
569	$1.14^{+0.08}_{-0.08}$	14^{+5}_{-3}	$3.1^{+0.6}_{-0.5}$	4.4×10^{43}	0.92	96
all data	$1.33^{+0.04}_{-0.04}$	18^{+7}_{-3}	$2.5^{+0.4}_{-0.6}$	4.4×10^{43}	1.04	268

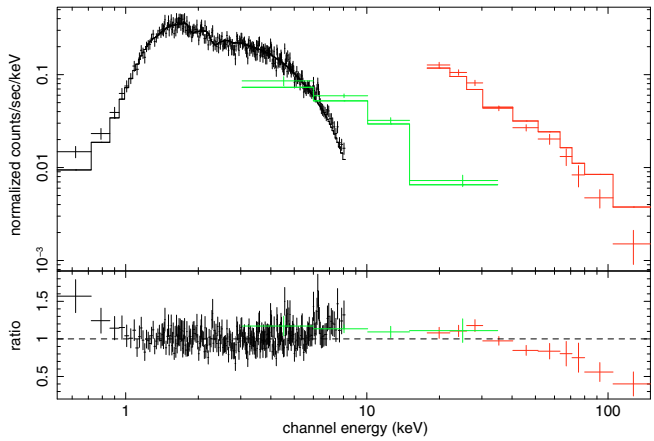

Fig. 4. Absorbed single power law model fit applied to the 2–5 keV range of the combined data set. The ratio between the data and the model shows the soft excess at energies below 1 keV, the iron Kα line, the significant cut-off at high energies, but no trace of a reflection component.

Similar values for cut-off energy and photon index as presented here were derived previously based on combined *BeppoSAX* and *INTEGRAL* IBIS/ISGRI data, resulting in $E_C = 112^{+40}_{-43}$ keV, $\Gamma = 1.74^{+0.08}_{-0.14}$, plus a reflection component with $R = 1.2^{+0.6}_{-1.0}$ (Molina et al. 2006). As these observations are not simultaneous, these values have to be taken with some caution though, and the reflection component is not well constrained.

Apart from the variation of the cut-off energy and of the plasma temperature, describing a variable inverse Compton process, the low level of the reflection component in the data studied here is remarkable. Figure 4 shows a simple model fit applied to the combined data set, using an absorbed power law model fitted in the 2–5 keV range as done by Reeves et al. (2007) to show the significance of the reflection component. The ratio between the data and the model shows several components: the soft excess at energies below 1 keV, the iron Kα line, and the significant cut-off at high energies. There is no evidence however of a significant reflection component.

The 2σ upper limit is $R < 0.25$, while in the observations presented by Reeves et al. (2007), a value of $R < 0.7$ can be excluded on a 3σ level. We have to conclude that the strong reflection component, visible in the December 2005 data taken by

Suzaku, *XMM-Newton* and *Chandra* disappeared within a year. Also the excess observed at soft X-rays by Reeves et al. is only detectable in the *Swift*/XRT data from December 2005 and not afterwards. At the same time, also the iron line complex has decreased in flux, from an equivalent width of $EW = 130 \pm 17$ eV in December 2005 to about $EW = 61 \pm 45$ eV in 2006/2007. Unfortunately the *Swift*/XRT data do not allow us to disentangle the broad and narrow line component of the line complex, as reported in Balestra et al. (2004) and also in Reeves et al. (2007). If we assume that the narrow and the broad line components arise from two different absorber, with the broad line being emitted closer and the narrow line further away from the central engine as proposed by Reeves et al., then we might indeed observe the disappearance of the broad iron line ($EW \simeq 60$ eV; Reeves et al. 2007) and of the reflection component connected to the close absorber between the December 2005 and December 2006 observations, leaving the spectrum only with the narrow line component and reflection from the distant absorber. This disappearance is not accompanied by a significant change in X-ray luminosity or in UV/optical flux. The lack of hard X-ray flux variability appeared also in a study of MCG–05–23–016 using *Swift*/BAT, which resulted in a marginal variability of $6 \pm 4\%$ on a 20 day time scale (Beckmann et al. 2007). The soft X-ray spectrum in the range 2–10 keV however appears to be variable by a factor of ~1.7 throughout historic observations. The *Swift*/XRT data presented here give a flux of $f_{2-10\ \mathrm{keV}} = (7.1 - 8.1) \times 10^{-11}$ erg cm^{-2} s^{-1}, with literature values in the range $f_{2-10\ \mathrm{keV}} = (7.1\text{–}11.9) \times 10^{-11}$ erg cm^{-2} s^{-1} (e.g. Mattson & Weaver 2004; Balestra et al. 2004).

Mattson & Weaver (2004) also found variable Compton reflection when studying MCG–05–23–016 with *RXTE* and *BeppoSAX*. In their study, the strength of the reflection component is anti-correlated with the 2–10 keV flux. In this context, one would expect a very high reflection component in the data presented here, where the 2–10 keV flux is at the historic minimum. When using the same photon index of $\Gamma = 1.77$ as Mattson & Weaver, we get a relative reflection of $R = 0.78^{+0.26}_{-0.21}$, but at the same time χ^2_ν rises to 1.10, compared to $\chi^2_\nu = 0.99$ with no reflection and a photon index of $\Gamma = 1.52$. We therefore do not consider the fixed spectral slope the valid approach to fit the data presented here. A similar behaviour, of a hardening of the spectra with decreasing reflection component as we see it from comparison with previous measurements, has been observed before. Zdziarski et al. (2004) analysed this relation for 61 *Ginga* observations of 24 radio quiet Seyfert galaxies. They found a strong correlation of the form $R = u\,\Gamma^v$ with the parameters $u = (1.4 \pm 1.2) \times 10^{-4}$ and $v = 12.4 \pm 1.2$. The observed trend follows closely this relation. Our measurement of $\Gamma = 1.5$ would result in $R = 0.03 \pm 0.04$, consistent with the upper limit we derived. Also the results of Mattson & Weaver and of Reeves et al. (2007) fit well on this correlation. The measurement of Molina et al. (2006) based on non-simultaneous *BeppoSAX* and *INTEGRAL* IBIS/ISGRI data however, with $R = 1.2$ and $\Gamma = 1.7$ lies about 7σ off this relation which results in $R = 0.13 \pm 0.16$. This might indicate that it is indeed essential to study simultaneous observations when determining the strength of the reflection component.

An inverted source behaviour in the sense that the strength of the reflection component is anti-correlated with the 2–10 keV flux might be another hint for a scenario in which the reprocessing occurs at large distance to the central engine of the AGN, and therefore a correlation of the reflected component and the continuum would appear with a large delay (Malzac & Petrucci 2002). Based on the data analysed here, this distance appears to be 1.5 light years, as there is no variability observable in the 2–100 keV X-ray luminosity, but significant variation in the reflection component. This would place the material relevant for the reprocessing at a distance of 0.55 pc, at the outer regions of the accretion disc. This being said, we cannot exclude that the flux varied in between the observations presented here, therefore the distance has to be taken as an upper limit.

3.2. Accretion power in MCG–05–23–016

MCG–05–23–016 presents a rather unique case. Its spectrum is, at least to the first order, nearly constant in shape and luminosity, with a possibly variable reflection component ($R = 0 \ldots 1$) and high energy cut-off ($E_C = 50 \ldots 120$ keV). The over all luminosity is low. Using the X-ray luminosity of $L_{2-200\ \mathrm{keV}} = 10^{44}$ erg s^{-1} as a proxy for the bolometric luminosity, the small black hole mass of $2 \times 10^6\ M_\odot$ (Whang & Zhang 2007) leads to a large Eddington ratio of $L_{\mathrm{bol}}/L_{\mathrm{Edd}} \gtrsim 0.4$. As the UV/optical emission is at least of the same order as the X-ray one, it is more likely that the Eddington ratio is as high as $L_{\mathrm{bol}}/L_{\mathrm{Edd}} \gtrsim 0.8$. Considering the error on the mass determination, this translates in a range of $L_{\mathrm{bol}}/L_{\mathrm{Edd}} = 0.2$–5.

An independent way to determine the mass of a black hole is to study its temporal behaviour. Following McHardy et al. (2006), the detection of a break in the X-ray power spectral density (PSD) of an AGN would allow to estimate the black hole mass thanks to the relation $T_{\mathrm{B}} = 2.1 \log(M_{\mathrm{BH}} \times 10^{-6}\ M_\odot^{-1}) - 0.98 \log(L_{\mathrm{bol}} \times 10^{-44}\ \mathrm{erg}^{-1}\ \mathrm{s}) - 2.32$. Using the data collected by *RXTE*/PCA and *XMM-Newton*/PN between 1996 and 2005, we estimated the X-ray PSD and structure function (*RXTE* data only) of MCG–05–23–016. The structure function has the advantage of working in the time domain and therefore being less sensitive to alias and windowing problems than the Fourier analysis. The PSD was calculated for each observation longer than 10 ks (on 200 s binned light curves), and the PSDs obtained were averaged and binned in logarithmically spaced bins (e.g. Uttley et al. 2002). The final PSD shows a flattening between 2×10^{-5}–10^{-4} Hz (10–50 ks), close to the minimum frequencies sampled by these data (~7×10^{-6} Hz). Also the structure function presents the hint of a break, but rather at ~3.5 ks. The lack of a longer-term monitoring prevents us from drawing a firm conclusion about the presence and the position of the break. Assuming a break in the range 0.04–0.6 days (3.5–50 ks), we achieve a black hole mass of $M_{\mathrm{BH}} = 1.84 - 3.3 \times 10^7\ M_\odot$. It has to be taken into account though that for the given bolometric luminosity the formula does not allow for black hole masses lower than $1.8 \times 10^7\ M_\odot$, even when the break time approaches zero. This means that it implies an upper limit for the Eddington ratio of $L_{\mathrm{bol}}/L_{\mathrm{Edd}} \lesssim 0.1$ at a luminosity of $L_{\mathrm{bol}} = 2 \times 10^{44}$ erg s^{-1}, which might be exceeded in the case presented here. It also means that the mass estimate of MCG–05–23–016 based on the temporal behaviour is at the lower limit of the possible values.

Figure 5 shows the SED of the source for the data presented here, corrected for Galactic absorption of $N_{\mathrm{H,Gal}} = 8 \times 10^{20}$ cm^{-2} in the line of sight, giving an extinction of $A_V = N_{\mathrm{H}}/1.79 \times 10^{21}$ cm^{-2} = 0.45 mag (Predehl & Schmitt 1995). The extinction in the UV is higher (e.g. $A_{\mathrm{U}} = 0.74$ mag), while the effect is insignificant in the near infrared with e.g. $A_K = 0.05$ mag (Schlegel et al. 1998). To the simultaneous data we added previous observations in the J, H, and Ks band from the 2MASS and VLA observations at 6 cm and 20 cm (Ulvestad et al. 1984) for comparison. The SED indicates that the bolometric

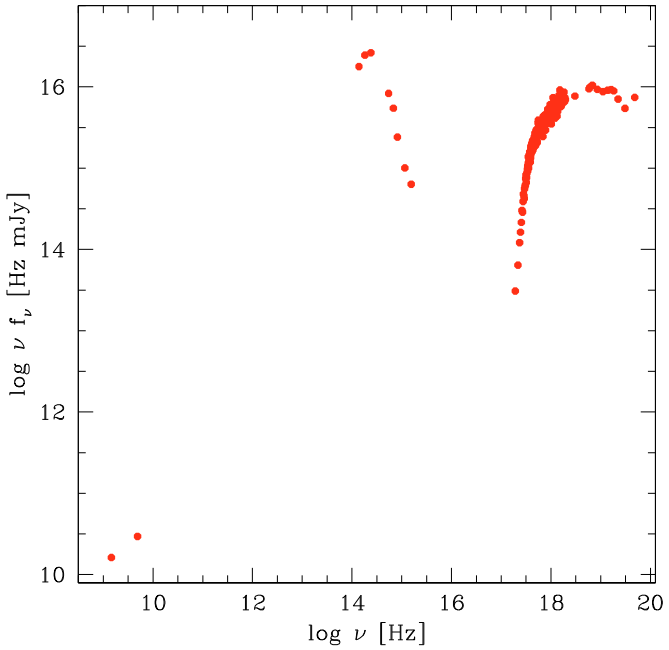

Fig. 5. Spectral energy distribution of the combined data set, including *Swift*/UVOT optical and UV data as well as *Swift*/XRT soft X-ray, and *INTEGRAL* JEM-X and IBIS/ISGRI hard X-ray data. In addition, 2MASS measurements (J, H, and Ks) and radio data (6 cm and 20 cm) have been added. Data have been corrected for Galactic hydrogen column density, but not for intrinsic absorption.

luminosity is probably $L_{\rm bol} > 2L_X$. Even considering the uncertainty of the mass determination, the source cannot be assumed to be a typical low-luminosity AGN, which exhibits Eddington ratios in the range 10^{-3} to 10^{-6} (Ho 1999), and the Seyfert 1.9 shows an Eddington ratio 10^8 times larger than that of Sgr A* which has a similar mass of $M = 3.3 \times 10^6\ M_\odot$ (Schödel et al. 2002). If we assume that the mass is in fact $M \lesssim 5\times10^6\ M_\odot$ then the Eddington ratio of $L_{\rm bol}/L_{\rm Edd} \gtrsim 0.8$ is also remarkable when compared to other Seyfert galaxies. Woo & Urry (2002) list a total of 32 Seyfert galaxies with black hole masses lower than $10^7\ M_\odot$ and only 3 of them have $L_{\rm bol}/L_{\rm Edd} \gtrsim 1$, whereas the average of these lower mass black holes is $L_{\rm bol}/L_{\rm Edd} = 0.30 \pm 0.05$. In the Galactic equivalent, the hard state is usually reached at small Eddington ratios, like $L_{\rm bol}/L_{\rm Edd} \simeq 10^{-3}$ in the case of XTE J1118+480 (Esin et al. 2001), and 0.003–0.2 for XTE J1550+564 (Done & Gierliński 2003). In fact the SED of the X-ray nova XTE J1118+480 in the low state appears very similar to the one of MCG–05–23–016. In XTE J1118+480 the thermal disc component has a temperature as low as 24 eV. Considering that the temperature scales with $T \propto M^{-0.25}$, the disc emission of the Seyfert can be expected at much lower frequencies and can be hidden in the SED component peaking around $10^{14.5}$ Hz. XTE J1118+480 also shows a power law component dominating the spectrum in the 0.4–160 keV range with a photon index of $\Gamma = 1.8$ (McClintock et al. 2001). The overall SED in this object can be explained by an advection dominated accretion flow (ADAF) model at 2% Eddington ratio Esin et al. (2001). Although the SED of MCG–05–23–016 appears to resemble the one of XTE 1118+480, its high Eddington ratio is unlikely to be arising from a radiative inefficient accretion as described in the ADAF. An object with higher Eddington ratio also in the hard state is GX 339-4, which reaches $L_{\rm bol}/L_{\rm Edd} = 0.25$ in the hard state in some cases before the state transition into the high-soft state (Zdziarski et al. 2004), consistent with MCG–05–23–016, although on average GX 339–4 reaches only an Eddington ratio of 0.015 and 0.05 during quiescence and during outburst, respectively. Considering a time scale for accretion rate changes in GX 339–4 of ~1000 days (Zdziarski et al. 2004), this would correspond to time scales of ~1 Myr in the case of MCG–05–23–016, as the variation times scale with the mass of the black hole.

Objects which are thought to exhibit extremely high Eddington ratios are the ultra-luminous X-ray sources (ULX). The true nature of these objects is still unclear though. Considering their luminosity, they are either intermediate mass black holes (IMBH) with a central mass as high as 100–100 000 $M_\odot$ (e.g. Colbert & Mushotzky 1999), or alternatively they are operating at very high Eddington ratio, as large as $L_{\rm bol}/L_{\rm Edd} > 20$ (Soria et al. 2007; Roberts 2007). ULX also show hard spectra and low temperature disc similar to XTE J1550–564 in very high state where the disc temperature decreases (e.g. Kubota & Done 2004). A study of *Chandra* data on ULX showed that the spectra can often be fitted by a simple power-law model, without evidence for thermal accretion disc components (Berghea et al. 2008), similar to MCG–05–23–016. In some cases ULX show a disc component, e.g. the *XMM-Newton* observation of two ULX in NGC 1313 revealed soft components which are well fitted by multicolor disc blackbody models with color temperatures of $kT \simeq 150$ eV.

An alternative model for the accretion process onto black holes has been proposed by Courvoisier & Türler (2005), in which the accretion flows consist of different elements (clumps) which have velocities that may differ substantially. As a consequence, collisions between these clumps will appear when the clumps are close to the central object, resulting in radiation. In the case of MCG–05–23–016, this model results in low-energetic collisions, which is also indicated by the missing variability in the UV band as seen by *Swift*/UVOT, where these collisions should cause flux variations.

Low mass AGN like MCG–05–23–016 operating at high Eddington rate might be an early state in the evolution towards high-mass black holes as seen in quasars. As the highest measured redshift of a quasar to date is $z = 6.43$ (Willott et al. 2007), we can assume that these objects with black hole masses of $M > 10^8\ M_\odot$ appear in the Universe around $z \sim 7$. If we assume the formation of the first heavy black holes with $M \sim 10^6\ M_\odot$ at redshift $z = 10$, we indeed need high mass accretion rates. An object like MCG–05–23–016, if we consider its mass to be indeed $M \lesssim 5 \times 10^6\ M_\odot$, with a constant Eddington ratio of $L_{\rm bol}/L_{\rm Edd} = 0.8$ and starting black hole mass of $M(z = 10) = 10^6\ M_\odot$ would reach a mass of $M(z = 7) = 4\times10^8\ M_\odot$. However, this would require not only the existence of a super massive black hole with $M \sim 10^6\ M_\odot$ at redshift $z = 10$, but also a high accretion rate over a time span of 3×10^8 yrs. But even at a duty cycle of only 20% for AGN activity at $z \geq 7$, objects like MCG–05–23–016 can evolve to $10^8\ M_\odot$, and it has to be taken into account that the duty cycle of AGN is likely to be larger in the high-redshift Universe (Wang et al. 2008). On the other hand, it has to be considered that the environment in which the AGN grows at redshifts $z > 7$ might be significantly different than the one we observe MCG –05–23–016 at in the local Universe.

4. Conclusions

The Seyfert 1.9 galaxy MCG–05–23–016 shows evidence for a variable reflection component, variable plasma temperature and high-energy cut-off energy. The combined data set presented here shows a low reflection component ($R < 0.3$) compared

to previous studies which show a value as high as $R = 1$. The data require a high-energy cut-off at 72 keV, but one observation shows an undisturbed power-law up to $E > 100$ keV. Tighter constraints on the hard X-ray spectrum and the effect of Compton reflection will be only achievable with focusing optics, as they will be provided by the future missions *Simbol-X*, *NuSTAR*, and *NEXT*.

During the observations the over all luminosity of the hard X-ray emission remained rather constant, as did the UV/optical emission. The spectral energy distribution shows similarities with the one of the X-ray nova XTE J1118+480 in the low-state with the peaks of the SED shifted according to what one would expect from a scaling of $T \propto M^{-0.25}$. While XTE J1118+480 is assumed to accrete at low efficiency, perhaps through an advection dominated accretion flow, the Seyfert core is likely to be in a radiative efficient state. The low mass of the central black hole implies that the accretion onto the central engine takes place at a high Eddington ratio. An equivalent in the Galactic black hole class appears to be GX 339–4 in hard state before state transition, although the efficiency of the accretion in MCG–05–23–016 is still higher. In this respect this source shows similarities to ULX. These high accretion flows are a key element in order to understand the rapid growth of black holes in the early Universe. Objects like MCG–05–23–016 might indicate the early stages of super massive black holes, in which a strong accretion flow feeds the central engine. With an Eddington ratio of $\gtrsim$0.8, objects like the one presented here can develop into quasars with 10^8 $M_\odot$, even considering a duty cycle of only 20%, within a time span of 3×10^8 yrs.

Acknowledgements. We thank the referee Chris Done who gave valuable advice which helped us to improve this paper. This research has made use of the NASA/IPAC Extragalactic Database (NED) which is operated by the Jet Propulsion Laboratory.

References

Arnaud, K. A. 1996, in Astronomical Data Analysis Software and Systems V, ed. G. Jacoby, & J. Barnes, ASP Conf. Ser., 17, 101
Balestra, I., Bianchi, S., & Matt, G. 2004, A&A, 415, 437
Beckmann, V., Barthelmy, S. D., Courvoisier, T. J.-L., et al. 2007, A&A, 475, 827
Berghea, C. T., Weaver, K. A., Colbert, E. J. M., & Roberts, T. P. 2008, ApJ, 687, 471
Braito, V., Reeves, J. N., Dewangan, G. C., et al. 2007, ApJ, 670, 978
Burrows, D. N., Hill, J. E., Nousek, J. A., et al. 2005, Space Sci. Rev., 120, 165
Colbert, E. J. M., & Mushotzky, R. F. 1999, ApJ, 519, 89
Courvoisier, T. J.-L., & Türler, M. 2005, A&A, 444, 417
Courvoisier, T. J.-L., Walter, R., Beckmann, V., et al. 2003, A&A, 411, L53
Dadina, M. 2007, A&A, 461, 1209
Done, C., & Gierliński, M. 2003, MNRAS, 342, 1041
Esin, A. A., McClintock, J. E., Drake, J. J., et al. 2001, ApJ, 555, 483
Gebhardt, K., Bender, R., Bower, G., et al. 2000, ApJ, 539, L13
Gehrels, N., Chincarini, G., & Giommi, P. 2004, ApJ, 611, 1005
Greene, J. E., & Ho, L. C. 2005, ApJ, 627, 721
Ho, L. C. 1999, ApJ, 516, 672
Ibragimov, A., Poutanen, J., Gilfanov, M., Zdziarski, A. A., & Shrader, C. R. 2005, MNRAS, 362, 1435
Kashlinsky, A., Arendt, R. G., Mather, J., & Moseley, S. H. 2005, Nature, 438, 45
Kubota, A., & Done, C. 2004, MNRAS, 353, 980
Lebrun, F., Leray, J. P., Lavocat, P., et al. 2003, A&A, 411, L141
Lund, N., Budtz-Jorgensen, C., Westergaard, N. J., et al. 2003, A&A, 411, L231
Magdziarz, P., & Zdziarski, A. A. 1995, MNRAS, 273, 837
Malzac, J., & Petrucci, P. O. 2002, MNRAS, 336, 1209
Mattson, B. J., & Weaver, K. A. 2004, ApJ, 601, 771
McClintock, J. E., Haswell, C. A., Garcia, M. R., et al. 2001, ApJ, 555, 447
McHardy, I. M., Koerding, E., Knigge, C., Uttley, P., & Fender, R. P. 2006, Nature, 444, 730
Miller, J. M., Fabbiano, G., Miller, M. C., & Fabian, A. C. 2003, ApJ, 585, L37
Molina, M., Malizia, A., Bassani, L., et al. 2006, MNRAS, 371, 821
Predehl, P., & Schmitt, J. H. M. M. 1995, A&A, 293, 889
Poutanen, J., & Svensson, R. 1996, ApJ, 470, 249
Reeves, J. N., Awaki, H., Dewangan, G. C., et al. 2007, PASJ, 59, 301
Roberts, T. P. 2007, Ap&SS, 311, 203
Roming, P. W. A., Kennedy, T. E., Mason, K. O., et al. 2005, Space Sci. Rev., 120, 95
Ross, R. R., & Fabian, A. C. 2005, MNRAS, 358, 211
Schlegel, D. J., Finkbeiner, D. P., & Davis, M. 1998, ApJ, 500, 525
Schödel, R., Ott, T., Genzel, R., et al. 2002, ApJ, 596, 1015
Soldi, S., Beckmann, V., Bassani, L., et al. 2005, A&A, 444, 431
Soria, R., Baldi, A., Risaliti, G., et al. 2007, MNRAS, 379, 1313
Titarchuk, L. 1994, ApJ, 434, 570
Tremaine, S., Gebhardt, K., Bender, R., et al. 2002, ApJ, 574, 740
Tueller, J., Mushotzky, R. F., Barthelmy, S. D., et al. 2008, ApJ, 681, 113
Ulvestad, J. S., & Wilson, A. S. 1984, ApJ, 285, 439
Uttley, P., & McHardy, I. M. 2004, PThPS, 155, 170
Uttley, P., McHardy, I. M., & Papadakis, I. E. 2002, MNRAS, 332, 231
Vedrenne, G., Roques, J.-P., Schönfelder, V., et al. 2003, A&A, 411, L63
Wang, J.-M., & Zhang, E. P. 2007, ApJ, 660, 1072
Wang, J.-M., Chen, Y.-M., Yan, C.-S., & Hu, C. 2008, ApJ, 673, L9
Willott, C. J., Delorme, P., Omont, A., et al. 2007, AJ, 134, 2435
Winkler, C., Courvoisier, T. J.-L., Di Cocco, G., et al. 2003, A&A, 411, L1
Woo, J.-H., & Urry, C. M. 2002, ApJ, 579, 530
Zdziarski, A. A., Lubiński, P., & Smith, D. A. 1999, MNRAS, 303, L11
Zdziarski, A. A., Gierliński, M., Mikołajewska, J., et al. 2004, MNRAS, 351, 791